GPS Solut (2018) 22:7
https://doi.org/10.1007/s10291-017-0667-9

ORIGINAL ARTICLE

Analysis and modeling GPS NLOS effect in highly urbanized area

Li-Ta Hsu[1]

Received: 10 January 2017 / Accepted: 13 October 2017 / Published online: 4 November 2017

Abstract Current GPS positioning accuracy in urban areas is still unsatisfactory for various applications, including pedestrian navigation and autonomous driving. Due to the ineffectiveness of special corrector designs against non-line-of-sight (NLOS) reception, the research regarding NLOS signals has been increasing in the recent years. This study first develops an algorithm to detect NLOS signals from the pseudorange measurements by using a 3D building model, ray-tracing simulation, and known receiver position. According to the analysis of 24 h of collected NLOS data, a new finding is that NLOS pseudorange delay is highly correlated with the elevation angle of satellite instead of the received signal strength. Thus, we further propose an innovative NLOS model using two variables, the elevation angle and the distance between the receiver and building that reflect the NLOS. The proposed model is evaluated in both pseudorange and position domains. Based on the experiment results regarding pseudorange error, the difference between the proposed model and the collected NLOS measurement is very small. Finally, the proposed model is applied to a hypothesis-based positioning method and achieves about 6.3 m in terms of horizontal positioning accuracy, which is only slightly worse than the method applied with ray-tracing simulation.

Keywords NLOS · Multipath · Urban area · Ray-tracing · Localization

✉ Li-Ta Hsu
lt.hsu@polyu.edu.hk

[1] Interdisciplinary Division of Aeronautical and Aviation Engineering, The Hong Kong Polytechnic University, Kowloon, Hong Kong

Introduction

The booming of transportation robotics such as unmanned aerial vehicle (UAV) and driverless car pushes the requirement of accuracy and precision of low-cost global navigation satellite system (GNSS) receivers. Multipath and non-line-of-sight (NLOS) receptions still are the main challenges for GNSS receiver in urban canyon (Groves 2013). Especially in Asian super urbanized cities such as Hong Kong and Tokyo, the challenges from the signal reflection at the dense skyscrapers further increasing the difficulty. Figure 1 shows the positioning data calculated by a commercial GNSS receiver, u-blox M8 receiver (GPS/Beidou mode), and collected in Kowloon, HK. Comparing the top and bottom panels of the figure, the positioning accuracy in urban area is much worse than that in the open area. It is evident the poor GNSS positioning result is caused by the GNSS signal blockage and reflection from the surrounding buildings.

Multipath and NLOS are different effects (Groves 2013), which are shown in Fig. 2. Multipath contains both the direct and reflected signals, while NLOS contains only the latter one. Even for a low-cost GNSS receiver, the multipath effect can be mitigated by sophisticated receiver correlator designs (Veitsel et al. 1998; Zhdanov et al. 2002). The principle of the correlator design is comparing the early, prompt and late channels in code tracking loop. In the other words, it compares the direct signal with reflected one. Unfortunately, this design does not mitigate the NLOS effect at all because the NLOS contains only the reflected signal. Thus, the research focused on detection and mitigation of NLOS is increasing. Detecting the NLOS using carrier to noise ratio (C/N_0) measurements of dual-polarization antenna is discussed in Jiang and Groves (2014). An advance tracking algorithm, i.e. vector tracking, has been proposed to detect and mitigate NLOS effect in signal processing stage (Benson 2007; Hsu

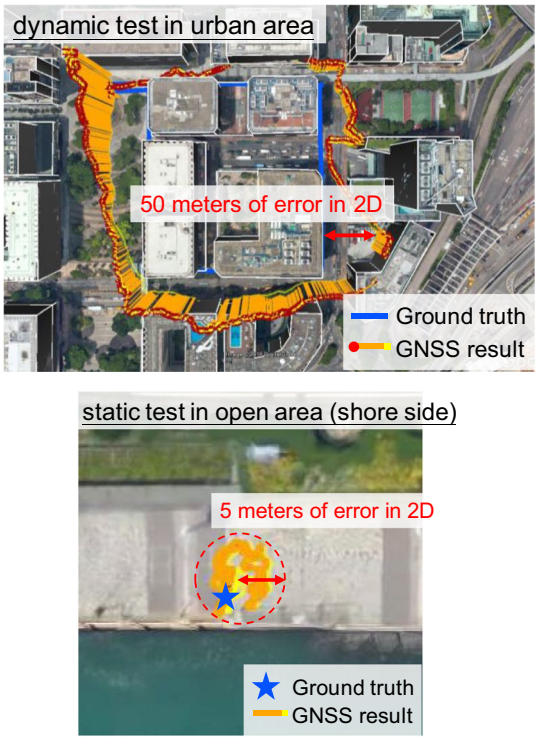

Fig. 1 Performance of a low-cost GNSS receiver obtained dynamically and statically from a quadcopter in the urban and open area of Kowloon, HK, respectively, on September 2016

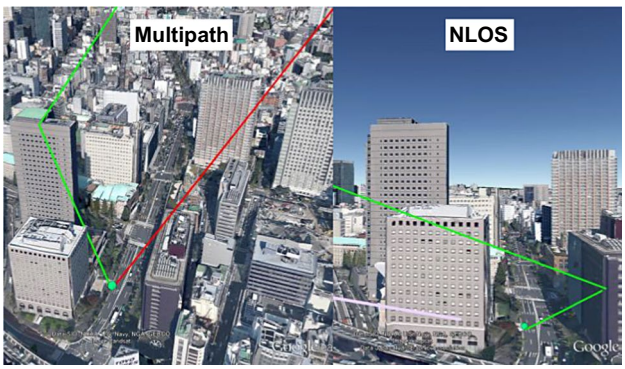

Fig. 2 Illustration of signal reception of multipath and NLOS effects (Hsu et al. 2016b)

et al. 2015; Kanwal et al. 2010). Consistency check between pseudorange measurements could detect and exclude large multipath and NLOS effects when the number of clean measurement is sufficient (Blanch et al. 2015; Groves and Jiang 2013; Iwase et al. 2013; Hsu et al. 2017). Another direction of study is to add other sensors to compensate the inaccurate GNSS positioning result caused by NLOS effect (Chiang et al. 2013; Gu et al. 2015; Han et al. 2015; Li et al. 2015; Sun et al. 2013; Wang and Gao 2010).

Due to the rise of smart cities, the 3D city models are rapidly developed and became widely available. Recent research dealing with multipath and NLOS utilizes 3D mapping and is called as 3D mapping aided (3DMA) positioning methods. Comprehensive related work on 3DMA positioning method can be found at Groves et al. (2015) and Breßler et al. (2016). One of the most well-known 3DMA methods is shadow matching proposed by university college London (UCL). It takes advantage of the 3D city model to generate building boundary in the Skyplot to help predicting satellite visibility (Groves 2011; Wang et al. 2012, 2013, 2015). The improvements of shadow matching in land, aviation, and mapping applications are deeply investigated by American and Israeli researchers (Yozevitch et al. 2014; Isaacs et al. 2014; Yozevitch and Ben-Moshe 2015). Researchers from the French institute of science and technology for transport (IFSTTAR) and the national higher French institute of aeronautics and space (ISAE-SUPAERO) also focused on improved GNSS positioning accuracy using enhanced 3D digital map (Ahmad et al. 2013; Betaille et al. 2013; Peyraud et al. 2013; Peyret et al. 2014). Instead of mitigating or excluding NLOS effect, in the past 3 years, the potential of using NLOS signal in constructive senses has been proposed. Researchers from Japan and Canada propose to combine ray-tracing simulation with hypothesis-based positioning method to further improve the positioning accuracy (Hsu et al. 2016b; Kumar and Petovello 2014; Miura et al. 2015; Suzuki and Kubo 2013). The range-based 3DMA uses a ray-tracing technique to estimate the reflection route of NLOS signal. The route is then used to correct the NLOS delay from the biased pseudorange measurement and it further improves positioning accuracy to about 5 m for pedestrian applications (Hsu et al. 2016a). However, the range-based method cannot be easily adapted to low-cost receiver due to (1) the heavy computational load caused by ray-tracing and (2) the inaccessibility to 3D building models in real time. The novelty and contribution of this research is to propose a NLOS model that can be used for hypothesis-based positioning without using ray-tracing in the low-cost devices.

To achieve the goal, the pseudorange error and its C/N_0 has to be investigated. In the stage of analysis, the NLOS is identified by a given ground truth of the receiver position and by 3D building models. Namely, it is identified if the ray-tracing simulation indicates that the building model obstructs the direct signal transmission path between satellite and receiver, and the receiver still receives it. To obtain the NLOS delay in the pseudorange domain, all the other errors are eliminated using differential GPS (DGPS) correction. 24 h of GPS raw data at an highly urbanized area is collected to retrieve the NLOS signals at different C/N_0 from different elevation angle. The result reveals an interesting finding. The pseudorange error caused by NLOS is highly correlated to elevation angle instead of C/N_0. This finding provides an inside view

for modeling NLOS delay as a function of elevation angle and distance from the receiver to the building that reflected the NLOS signal. Note that the distance can be roughly given according to different applications.

The detection of NLOS signal and its delay in pseudorange domain is given first. Analysis of 24-h NLOS data is conducted next, followed by a description of the innovation NLOS pseudorange error model proposed here, and the experimental setup and results. Finally, the conclusions and future work are summarized.

Estimation of NLOS delays in the pseudorange domain

NLOS pseudorange measurement deteriorate by delays including tropospheric errors, ionospheric errors, satellite clock/orbit bias, receiver clock bias, and our target NLOS. Other errors must be eliminated before the NLOS analysis. DGPS and least square estimation (LSE) are used to deal with former and latter part of the errors, respectively.

Differential GPS correction

DGPS is a mature technique (Misra and Enge 2011). A reference station is installed to receive the GPS measurements. The position of the reference station is precisely surveyed. After generating DGPS correction, the correction is transmitted to rover. The rover then applies it to the common satellites in view to enhance its own positioning accuracy. The differential correction can be generated by calculating the difference between the raw pseudorange and true (geometric) range for a satellite. Multipath and NLOS effects to the reference station are usually negligible because the open-sky environment and the geodetic antenna with choke-ring design as shown in the right panel of Fig. 3. Theoretically, DGPS correction is capable of eliminating satellite clock/orbit, tropospheric, ionospheric errors if the distance between the reference and rover stations is within 100 km. This research uses HKSC station of SatRef, which is a network of GNSS reference stations established by the land department of HK government as shown in Fig. 3. The distance between each reference station is less than 20 km. By the use of its archived RINEX 3.02 data that are free to HK publics, the differential correction can be easily generated.

Receiver clock bias and thermal noise

After applying the DGPS correction to pseudorange measurement, its receiver clock bias and thermal noise are still required to be corrected. The general LSE uses multiple (at least 4) measurements to estimate four unknowns including horizontal, vertical position and receiver clock bias as per equation:

$$\hat{\mathbf{x}} = \begin{bmatrix} \hat{x} \\ \hat{y} \\ \hat{z} \\ \hat{b} \end{bmatrix} = (\mathbf{G}^{\mathrm{T}}\mathbf{G})^{-1}\mathbf{G}^{\mathrm{T}}\tilde{\boldsymbol{\rho}} \tag{1}$$

where $\hat{x}, \hat{y}, \hat{z}$ represent the estimated receiver position in latitude, longitude and altitude directions and the $\hat{b}$ is the receiver clock bias in meters. $\mathbf{G}$ is the geometry matrix, containing the unit line-of-sight (LOS) vectors from satellites to receiver. $\tilde{\boldsymbol{\rho}}$ denotes the measured pseudoranges corrected by DGPS correction. An approach to better estimate the receiver clock bias is to reduce the unknown $\hat{x}, \hat{y}, \hat{z}$. The receiver is set statically in the experiment so that the ground truth of receiver position can be easily determined. The ground truth is given by the topographic map available from land department of HK government. The resolution of the map is 20 cm. Each point is given with accurate 2D coordinate. The height is given by the topography height obtained from Google plus the height of equipment. Thus, the only unknown left in the LSE is the receiver clock bias as per equation:

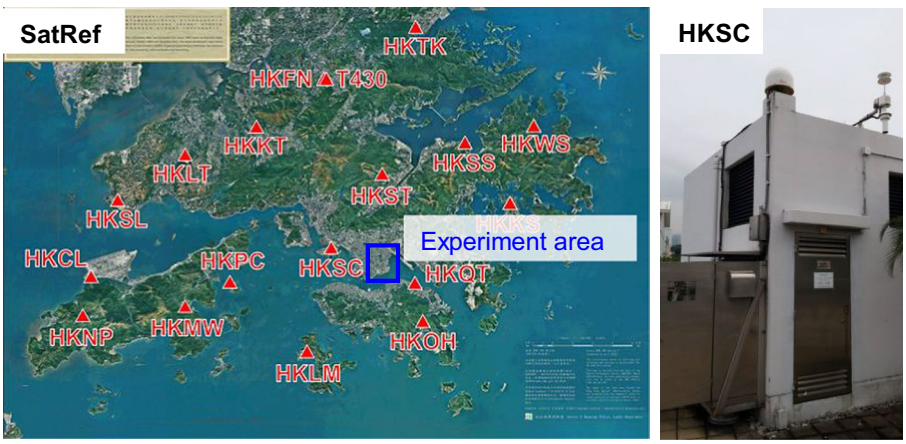

Fig. 3 Distribution of SatRef stations around HK and antenna and environment of HKSC station

$$\hat{b} = (\mathbf{G}^{\mathrm{T}}\mathbf{G})^{-1}\mathbf{G}^{\mathrm{T}}\tilde{\rho} \tag{2}$$

However, if the multipath and NLOS biased measurements are used, the estimated receiver clock bias will be contaminated. A clean, namely LOS, measurement identification is therefore required. Two criteria are used to identify the measurement type, and they are the C/N_0 ratio and the signal type determined by ray-tracing simulation. In general, the C/N_0 of LOS is larger than that of multipath and NLOS. A 40 dB-Hz threshold of C/N_0 is set empirically. The possible signal transmission type can be categorized as

$$\text{ray} \in \{\text{LOS, NLOS}\} \tag{3}$$

by the use of ray-tracing. The algorithm of rough LOS identification through ray-tracing is as follows:

if a measurement has C/N_0 larger than 40 dB-Hz and it is identified as LOS by ray-tracing, the measurement will be used to calculate the receiver clock bias. The receiver thermal noise is neglected because it is much smaller than the effect of NLOS. Finally, the NLOS delay in pseudorange domain, $\Delta\rho_{\mathrm{NLOS}}$, can be calculated as,

$$\Delta\rho_{\mathrm{NLOS}} = \rho - \left(R^{\mathrm{rcv}} + \rho^{\mathrm{Corr}} + \hat{b}\right), \quad \forall\rho \in \mathrm{NLOS} \tag{4}$$

where ρ denotes NLOS pseudorange measurement, R^{rcv} denotes line of sight distance between the satellite and receiver position and ρ^{Corr} denotes the DGPS correction. The analysis of the $\Delta\rho_{\mathrm{NLOS}}$ is detailed in the next section.

The detection of NLOS is simply based on the result of ray-tracing simulation from the given ground truth of

Algorithm 1: LOS identification for a measurement using ray-tracing simulation	
STEP1:	Prepare a line segment connecting the receiver and the satellite of the measurement (i).
STEP2:	initialize signal type of measurement (i) as LOS, $ray^{(i)} = LOS$
STEP3:	**for all** the building model $\mathbf{B}^j$ **do**
STEP3:	**for all** planes (walls) $\boldsymbol{w}_k^j$ of a building **do**
STEP4:	**if the** intersection between the line segment and plane w_k^j exists **then**
STEP5:	the measurement identified as NLOS, $ray^{(i)} = NLOS$
	break
	end if
STEP6:	**end for** planes
STEP7:	**end for** buildings

I

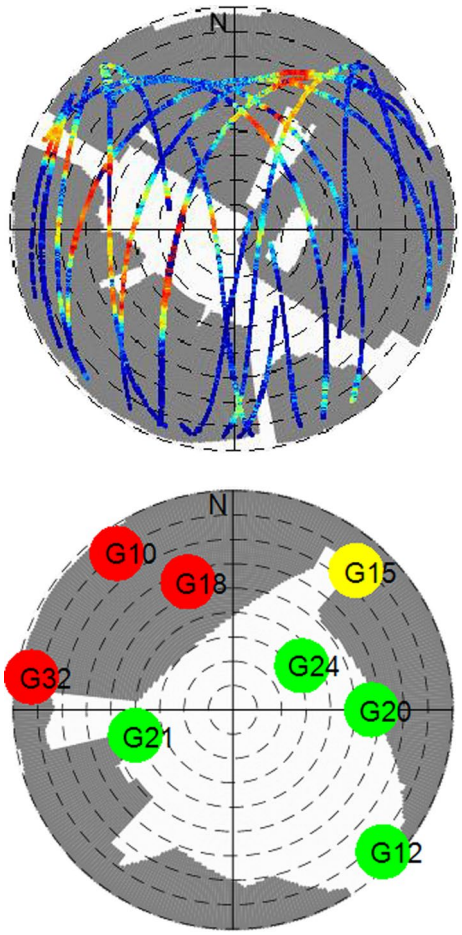

Fig. 4 Skyplots with surrounding building information of data collected in Kowloon. In the top panel, the color of satellite trajectory denotes C/N_0, the redder the color the higher is the C/N_0 received. In bottom panel green, red and yellow indicate LOS, NLOS and multipath signal, respectively

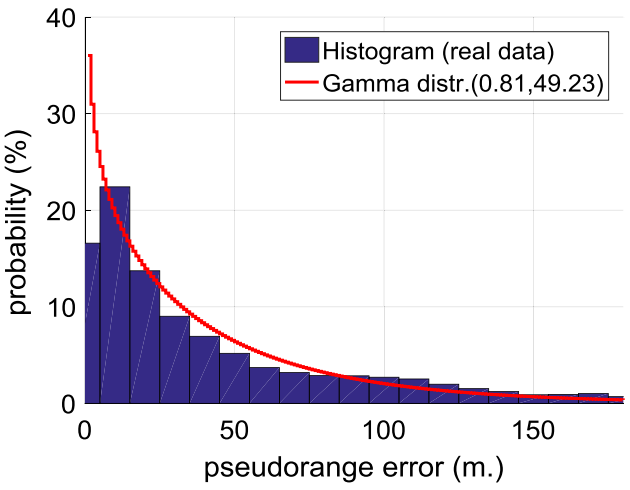

Fig. 5 Histogram of NLOS delays in pseudorange domain. The total number of NLOS signal received is 128,054

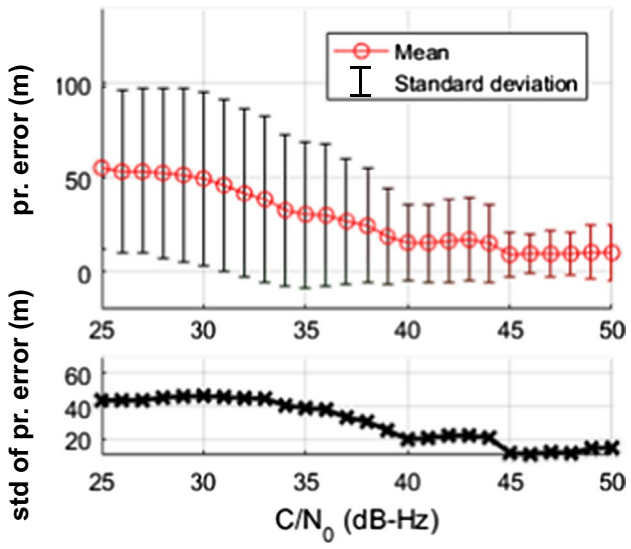

Fig. 6 Mean and standard deviation of NLOS pseudorange error with respect to carrier to noise ratio

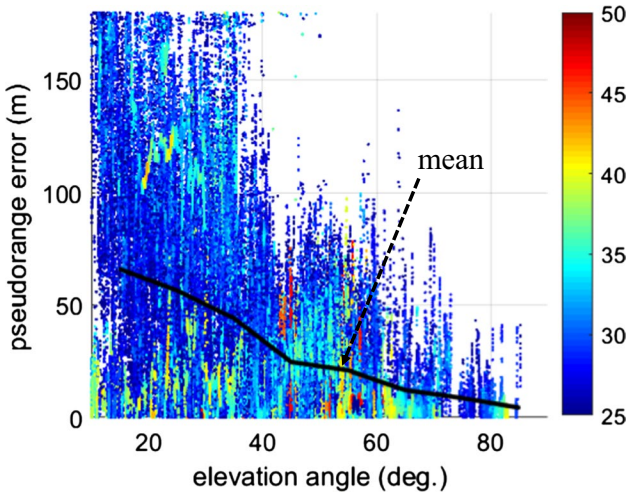

Fig. 7 NLOS pseudorange error with respect to elevation angle of the 24-h data. The color denotes the carrier to noise ratio of each point

receiver position. The NLOS is identified if the LOS path between the satellite and receiver is blocked, but the receiver still receives it.

NLOS data analysis

Low-cost u-blox M8 receivers are used to record pseudorange measurements. A 3D building model with level of detail (LOD) 1 used in this research is obtained from land department of the HK government. Two data are collected at different locations of urban area of Kowloon, HK. The

first and second data consists of 24 h and 30 min of GPS pseudorange measurements, respectively. Figure 4 shows the skyplot of data 1 and 2. As shown in the figure, many signals can be received even if its LOS transmission path is obstructed. In the following analysis, only the identified NLOS signal is evaluated.

NLOS data 1: case of 24 h

There are 128,054 NLOS measurements detected in the 24-h data from different satellites as demonstrated in the top panel of Fig. 4. Figure 5 shows the histogram of NLOS delays in the pseudorange domain.

The probability density distribution (PDF) of Fig. 5 exhibits the probability of an observed NLOS resulting in a corresponding pseudorange error. As shown in the figure, more than 70% of the NLOS delay is less than 50 m. Note that this PDF cannot show the probability of an unknown measurement with a certain pseudorange error to be a NLOS measurement. It is evident that NLOS delay cannot be modeled as Gaussian distribution. By the use of maximum likelihood function, the probability density distribution of NLOS delay can be described as a Gamma distribution:

$$f(x|k=0.81,\ \theta=49.23)=\frac{1}{\Gamma(k)\theta^k}x^{k-1}e^{-\frac{x}{\theta}}, \tag{5}$$

where $\Gamma(\cdot)$ denotes the Gamma function. Its non-Gaussian property shows the difficulty of mitigating NLOS effect. As suggested in the popular weighting model, the sigma-ϵ model (Hartinger and Brunner 1999), the signal strength is a hint to indicate the quality of pseudorange measurement. Figure 6 shows the relationship between NLOS delay with respect to C/N_0. The mean of NLOS error slowly decreases as the C/N_0 increases. Its standard deviation follows the same trend. This figure roughly verifies the reason that using the sigma-ϵ model in weighted LSE can improve the GPS positioning result in many cases even in urban canyon.

Error sources, such as atmospheric and multipath effects, are correlated with elevation angle. In general, they monotonically increase as elevation angle decreases as described in the conventional elevation angle-based weighting model (Special-Committee-159 2001). Figure 7 shows the relationship between NLOS delay with elevation angle. It is clear that the NLOS decreases as the elevation increases, in the other words, using the conventional elevation model in weighted LSE is also able to mitigate the NLOS effect. As shown in the figure, when the elevation angle is between 10° and 20°, its C/N_0 is usually lower than 30 dB-Hz. This phenomenon proves the agreement that both applying C/N_0 or elevation angle-based weighting models can improve GPS positioning when NLOS signal is present. However, it is not necessary that the lower the elevation angle is, the lower the carrier to noise ratio is. Figure 8 shows the different behaviors between the received signal strength of LOS and NLOS using the same commercial GNSS receiver. As shown in the figure, the mean of C/N_0 of LOS increases as the elevation increases. Its standard deviation decreases as the elevation increases. In the other words, the quality of LOS is more stable at higher elevation angle. The NLOS data shows a very different behavior. As the elevation increases, the C/N_0 does not increase following the behavior shown in the data of LOS. The standard deviation of NLOS C/N_0 also does not show the obvious tendency with elevation variation. The reason is that the NLOS is a reflected signal. The material of the reflecting surface can greatly change the signal strength of reflected signals. Comparing the top and bottom panels, one might conclude that C/N_0 could be used to distinguish the LOS or NLOS signal as the elevation angle increase. This conclusion is similar to the finding in Yozevitch et al. (2016) on LOS/NLOS classification using machine learning approach.

The statistic of a large amount of data can reveal the general characteristic of NLOS delay. It will be interesting to study whether short data would comply with the summarized characteristics or not.

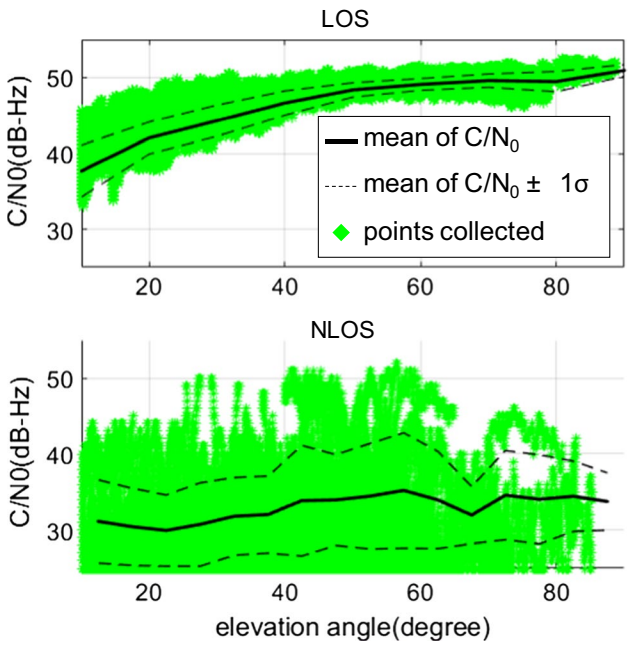

Fig. 8 Comparison of LOS and NLOS in terms of C/N_0 with regards to elevation

NLOS data 2: case of 30 min

In the 30-min data, there are 1648 NLOS measurements detected from three different satellites as shown in the bottom panel of Fig. 4. There are 4 LOS, 3 NLOS and 1 multipath signal in this case. Similar analysis is conducted to the

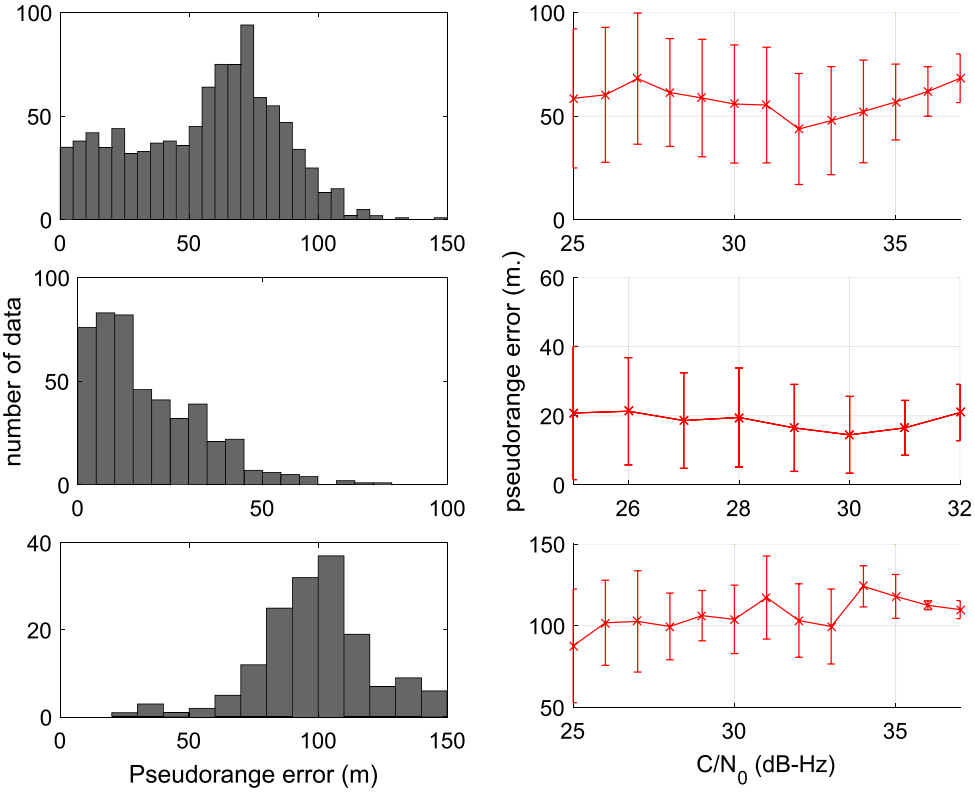

Fig. 9 Three NLOS signals from different satellite are collected. Left panel denotes histogram of NLOS delay and right panel denotes mean and standard deviation of NLOS pseudorange error with respect to carrier to noise ratio of the 30-min data

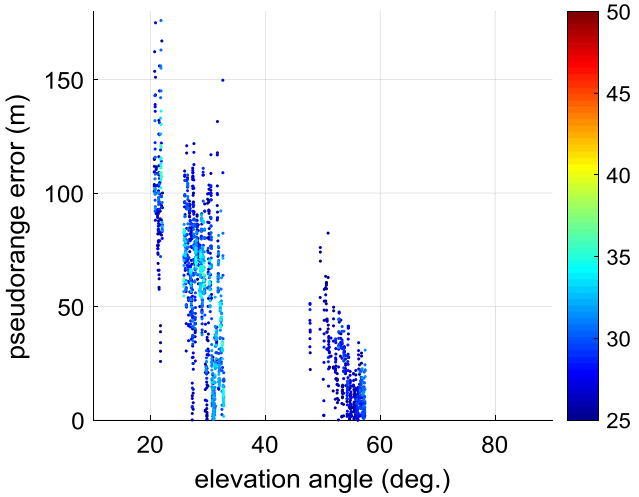

Fig. 10 NLOS pseudorange error with respect to elevation angle of the 30-min data. The color denotes the carrier to noise ratio of each point

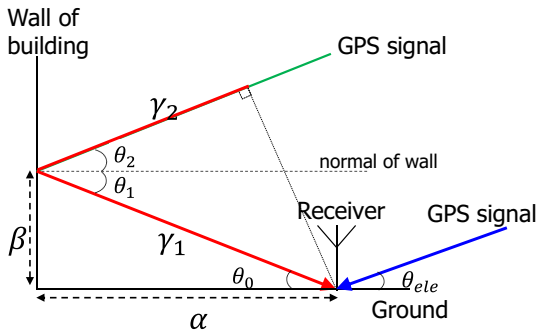

Fig. 11 Illustration of a reflecting signal that followed the law of reflection

30-min data as shown in Figs. 9 and 10. To observe Fig. 9, the NLOS pseudorange delay does not decrease as the C/N_0 increases. Instead, it remains a similar delay with different C/N_0. Interestingly, the pseudorange delay is still correlated with the elevation angle as shown in Fig. 10, namely the higher elevation angle, the smaller the NLOS pseudorange. Based on the principle of the GPS signal tracking loop, the effect of NLOS is different from multipath. For NLOS, only the delayed (reflected) signals comes into the receiver, which could easily deceive the receiver that the NLOS signal is LOS signal. According to the algorithm of estimating C/N_0 (Sharawi et al. 2007), the carrier strength is calculated by accumulating the power of I and Q channels. If NLOS signal are continuously present in the environment, its C/N_0 could also be strong. Thus, the strong C/N_0 is not necessary indicating a clean measurement. It could still contain tens of meters of pseudorange error. The previously obtained characteristic from the 2-h data of NLOS delay varying with C/N_0 is due to the C/N_0 being correlated with the elevation angle. In fact, C/N_0 could increase

as the elevation angle increased because of the longer signal transmission path and the pattern of antenna gain. As a result, it can be concluded that elevation angle is a dominant factor to NLOS pseudorange errors.

Modeling of NLOS

This section tries to derive a model to represent NLOS delay using the dominant factor, i.e. the elevation angle, previously verified. In highly urbanized areas, most of the buildings use excessive glass windows as a face of modern architecture. We, therefore, assume the GPS signal reflection follows the law of reflection to model the NLOS signal. An illustration of a perfect reflecting signal received by a receiver is given in Fig. 11.

The blue line represents a LOS signal. Green and red lines are the reflecting signal. Due to the distance between satellite and receiver is large compared to the distance between the LOS and reflecting signals, the blue line is not only parallel to the greens but also same length. Therefore, the NLOS delay (γ) in the pseudorange domain is the red lines:

$$\gamma = \gamma_1 + \gamma_2 \tag{6}$$

where γ_1 and γ_2 are:

$$\gamma_1 = \alpha \sec \theta_0 \tag{7}$$

$$\gamma_2 = \gamma_1 \cos(\theta_1 + \theta_2) \tag{8}$$

where α denotes the distance between the receiver to the obstacles (buildings) that reflected the navigation signal. Angle of reflection θ_1 equals to the angle of incidence θ_2 because the law of reflection is assumed. In addition, since the green and blue lines are parallel, θ_1 and θ_0 are alternate interior angles, namely $\theta_1 = \theta_0$. Assuming the wall of building is perpendicular to the ground, thus the normal of wall is parallel to ground resulting $\theta_2 = \theta_{\text{ele}}$. θ_{ele} denotes the elevation angle of the satellite. Finally, $\theta_{\text{ele}} = \theta_2 = \theta_1 = \theta_0$; thus, the NLOS delay can be represented as:

$$\gamma = \alpha \sec \theta_{\text{ele}} \left(1 + \cos 2\theta_{\text{ele}}\right) \tag{9}$$

In (9), only the distance between the receiver to the obstacle is unknown to a GPS receiver. Fortunately, this distance α could be roughly obtained from the 2D maps that are widely available to vehicle navigator and pedestrian with smartphone. According to road planning standards and guidelines of HK government, the general road width for primary and district distributor is between 6.75 and 13.5 m (HKPSG 2016). The path width of pedestrian walk is between 3.5 and 4.5 m (HKPSG 2016). Thus, a proper value of α in HK will be from 3.5 to 18 m for vehicle applications. For the autonomous driving, the LiDAR sensor will provide the distances between vehicle and buildings, which can be used by the proposed NLOS model.

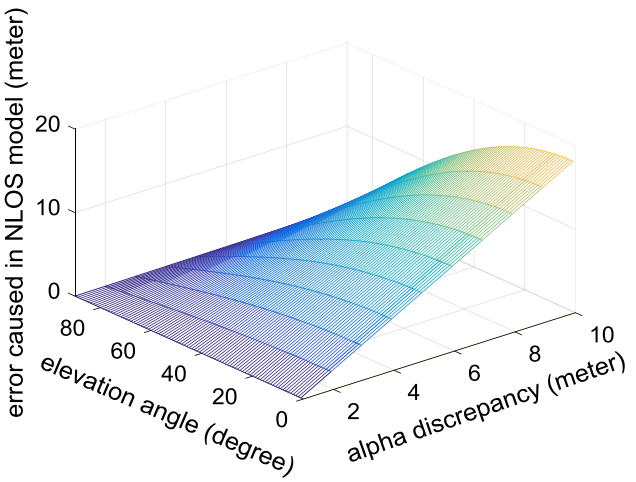

Fig. 12 Pseudorange error caused in the proposed NLOS model if alpha is not accurate

Fig. 13 NLOS can be frequently observed in typical urban residential area in Asian urbanized city. The left panel denotes the environment that the data were collected, and right panel indicates the installment of the path antenna

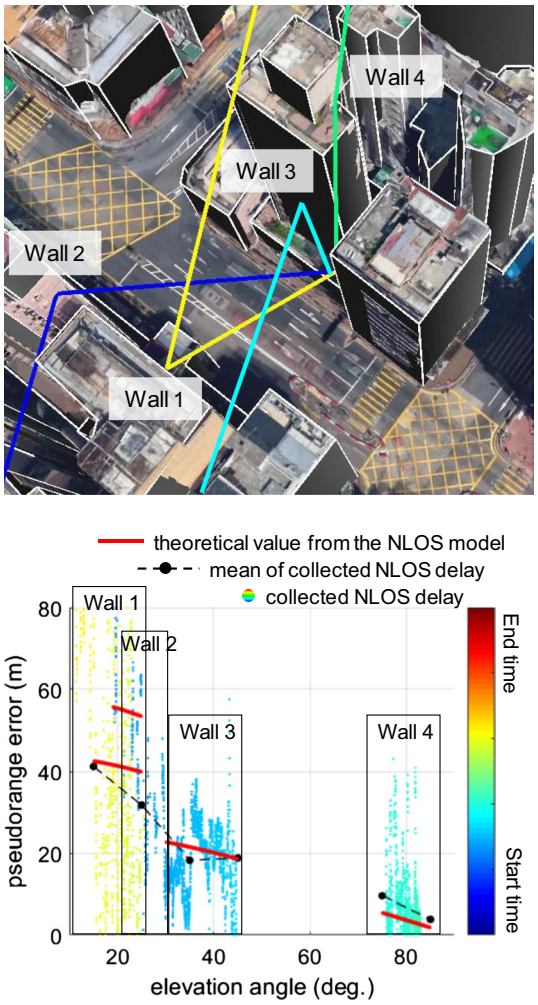

Fig. 14 Example of a received NLOS signal. Top panel demonstrates signal traveling paths reflected at four different walls by ray-tracing simulation, and bottom panel shows the NLOS delay of SV 27 that travelled from 0° to 85° of elevation angle

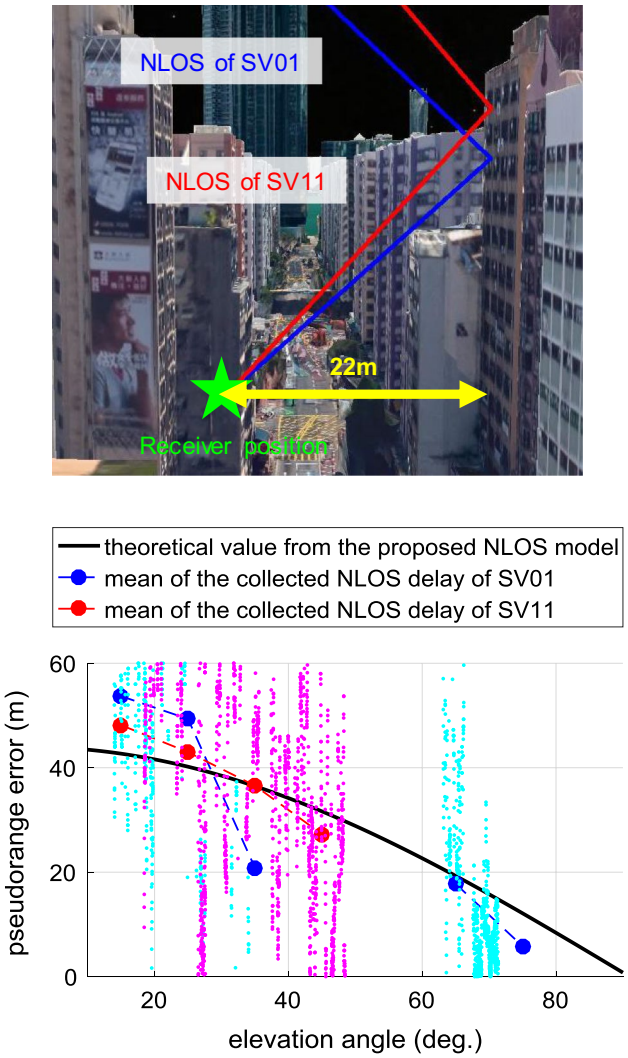

Fig. 15 Example of the two received NLOS signals reflected at same building. Top panel shows the ray-tracing simulation of NLOS from SV01 and SV11 reflected at Wall 1. Bottom panel shows the collected NLOS delay and theoretical value calculated by the proposed model

Considering an example, the alpha will be set to 18.2 m based on the map information, but alpha measured by LiDAR is 15.6 m. In the case of elevation angle of 61.6° and the alpha discrepancy of 2.6 m, the error introduced to the proposed NLOS model is 2.5 m. To further discuss other cases, a simulation of error introduced under different elevation angle and alpha discrepancy is shown in Fig. 12. As can be seen, the newly introduced error is smaller the higher of elevation angle and smaller the alpha discrepancy.

Experiment result

A commercial GPS receiver, u-blox M8, is deployed to collect NLOS data. Two different locations at a highly urbanized city are selected to evaluate the performance of the proposed NLOS model in pseudorange and position domains, respectively.

Verification of the NLOS model in pseudorange domain

In order to evaluate the proposed model in different elevation angle, a long-time data with NLOS signal must be collected. Figure 13 demonstrates the environment that the data were collected. The antenna is attached with a stick and put outside of the window for long-time data collection.

Figure 14 shows an example that the NLOS signal from a same satellite that travelled from 0° to 85° of elevation angle.

The x-axis of the bottom panel of Fig. 14 is the elevation angle of measurement, and the y-axis is the NLOS

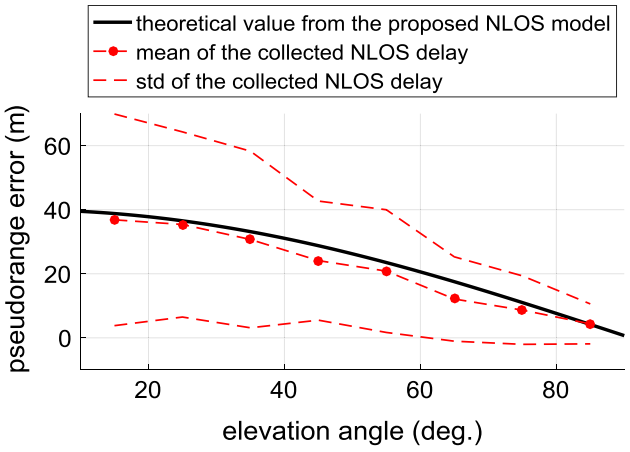

Fig. 16 Mean and standard deviation of all the NLOS delays reflected at Wall 1 from different SVs

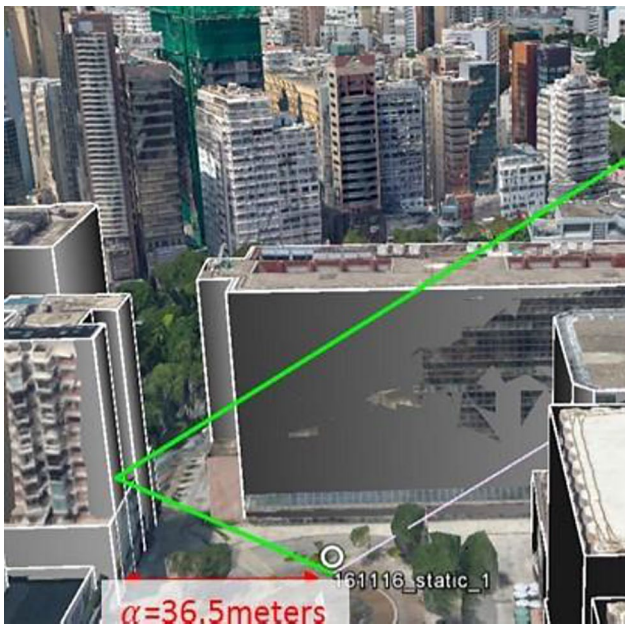

Fig. 17 Ray-tracing simulation of the static experiment

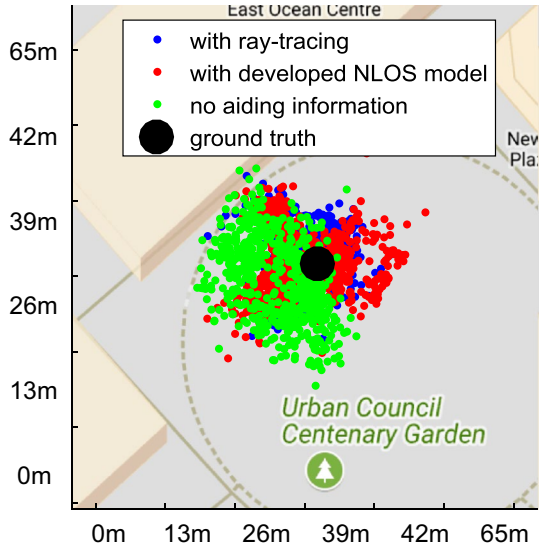

Fig. 18 Result of hypothesis-based positioning method using 3D building mode, the proposed NLOS model and no aiding information

Table 1 Positioning performance of hypothesis-based positioning method using ray-tracing, the proposed NLOS model and no aiding information

Methods	Mean (m)	SD (m)
Ray-tracing	5.05	2.99
Proposed NLOS model	6.27	3.31
No aiding information	8.67	3.93

delay in pseudorange domain calculated by (5). The black dashed line denotes the mean of the collected NLOS delay of different elevation angle (with a resolution of 10°). The trend of the collected NLOS delay decreases as the elevation increases. It is clear that the signal transmission path of SV 27 was not blocked during the elevation angle between 45° and 75° as shown in the bottom panel. The color of each point denotes the time of recording data, the bluer the point is earlier that signal is collected. The NLOS reflections of SV 27 are caused by four different buildings as shown in the top panel. Thus, the NLOS delays can be separated into four different groups. The red solid lines of the bottom panel denote the theoretical NLOS delay calculated from the proposed model. The distances between the receiver and the walls (α) are about 22, 29.5, 13.1 and 10.5 m for Wall 1 to 4, respectively. As can be seen from the bottom panel, the theoretical values are similar to the mean of collected values (with a region of 10 m), expecting reflection from Wall 2. In fact, during the elevation angle from 20° to 30°, the receiver has a great possibility to receive multiple NLOS signals simultaneously. This effect is called *multipathing NLOS*, which is complicated to model due to the undisclosed tracking correlator design of commercial receiver. To better verify the proposed model, signals reflected at the same wall but from different satellites are preferred. Most of the reflections of the long-time collected data come from Wall 1 shown in the top panel.

Figure 15 shows the cases of the other two satellites, SV01 and SV11, that only reflected at Wall 1. The black solid line of bottom panel denotes the NLOS delay calculated from the proposed model. Even through the data is noisy, the mean of NLOS delay is still close to the proposed model. This result verifies that if the NLOS is a single refection from a wall, the proposed model can predict the NLOS delay. All the NLOS reflected at Wall 1 from different SVs is organized in Fig. 16.

The theoretical value calculated from the proposed NLOS model, namely (9), is very close to the mean of the data. In the other words, the proposed method can obtain the mean of NLOS but not the standard deviation. Interestingly, the standard deviation of the data decreases as the elevation angle increases because the lower the elevation angle is, the lower the C/N_0 is obtained.

Positioning method using hypothesis-based positioning method

A static experiment is conducted in the environment shown in Fig. 17. Many glassy buildings are surrounded to the receiver. A measurement with NLOS reflection is detected and simulated in the figure. The distance between the building and receiver is about 36.5 m.

To apply the proposed NLOS model, the position of receiver is essential. The previous work proposes a position hypothesis-based positioning method (Hsu et al. 2016b). This approach distributes several position candidates and gives them proper weighting by evaluating their pseudorange similarities between the ray-tracing results and measurements. This positioning method is used to evaluate the NLOS model proposed. The NLOS pseudorange delay based on ray-tracing is replaced as the NLOS model. The rest of algorithm is the same. The positioning results of the hypothesis method using ray-tracing, the NLOS and without any aiding information is demonstrated and evaluated in Fig. 18 and Table 1. Only the data with the identified NLOS measurement is evaluated. It is important to note that NLOS identification is required in the hypothesis-based positioning method. The three methods evaluated above used 3D building models to determine the signal type of each measurements. It is evident that the method with ray-tracing simulation certainly obtained the best performance among the three methods, which is about 5 m of horizontal positioning accuracy. However, its computational load is also much higher than that of the other two. The hypothesis-based method using the proposed NLOS model achieves 6.27 m of accuracy, which is slightly worse than the method with ray-tracing. If no any aiding information used to correct the NLOS measurements, the positioning accuracy is about 8.67 m. This result verifies the proposed NLOS model is capable of replacing the use of ray-tracing in calculating NLOS delay in the pseudorange domain.

Conclusions and future work

Multipath interference and NLOS reception are major error sources when using GNSS positioning in urban environments. We first analyze a long-time GPS NLOS data and summarize as follows (1) the NLOS delay is not fitted to Gaussian distribution. Instead, it is more similar to a gamma distribution; (2) mitigating NLOS effects by given weighting based on C/N_0 could be incorrect; (3) NLOS delay is highly correlated to the elevation angle. The second contribution is to propose an innovative NLOS model. The NLOS model is based on the elevation angle and the distance between the receiver and the building that reflected the NLOS signal. If the distance can be appropriately selected, the proposed model can accurately describe the NLOS delay of the measurements. The effectiveness of the proposed model is demonstrated by applying it into a hypothesis-based positioning algorithm. The experiment result shows the positioning error only to increase about 1.3 m after replacing the NLOS delay, estimated by ray-tracing, into the proposed model in the particle filter-based positioning algorithm.

However, this result still applies the ray-tracing to identify whether the measurement is LOS or NLOS. Concerning the practical use of the proposed NLOS model, it requires working with other NLOS detection algorithms. To reduce the computational load, we provide three suggestions to integrate with the proposed NLOS model. (1) Using additional memory space: an ideal approach is to integrate the proposed NLOS model with shadow matching positioning algorithm (Groves 2011), which only applies the building boundary (using only memory). (2) Benefiting from Big Data era: another promising and innovative approach is to implement LOS/NLOS classifier trained by unsupervised/supervised machine learning algorithm before applying the proposed NLOS model. As suggested in Yozevitch et al. (2016), their decision tree-based robust classifier achieves over 85% of accuracy of NLOS detection. (3) Increasing the instrument cost: alternatively, a dual-polarization antenna can be implemented in the localization system to effective detect NLOS reception (Jiang and Groves 2014).

An interesting future work could be modeling the residue of multipath effect after applying sophisticated correlator design. The nature of multipath effect is very different with NLOS reception. To study the multipath residue, a software receiver is required to take the advantage of its flexibility to alter the correlator design of code tracking loop.

Acknowledgements Funding was provided by Hong Kong Polytechnic University (HK) (Grant No. 1-ZVKZ).

References

Ahmad KAB, Sahmoudi M, Macabiau C, Bourdeau A, Moura G (2013) Reliable GNSS positioning in mixed LOS/NLOS environments using a 3D model. In: European Navigation Conference (ENC), Vienne, Austria, Apr 2013, pp 1–9

Benson D (2007) Interference benefits of a vector delay lock loop (VDLL) GPS receiver. In: Proceedings of ION AM 2007, Institute of Navigation, Cambridge, Massachusetts, USA, 23–25 Apr, pp 749–756

Betaille D, Peyret F, Ortiz M, Miquel S, Fontenay L (2013) A new modeling based on urban trenches to improve GNSS positioning quality of service in cities. IEEE Intell Transp Syst Mag 5:59–70

Blanch J, Walter T, Enge P (2015) Fast multiple fault exclusion with a large number of measurements. In: Proceedings of ION ITM 2015, Dana Point, California, USA, 26–28 Jan 2015, pp 696–701

Breßler J, Reisdorf P, Obst M, Wanielik G (2016) GNSS positioning in non-line-of-sight context-a survey. In: 2016 IEEE 19th international conference on intelligent transportation systems (ITSC), 1–4 Nov 2016, pp 1147–1154

Chiang K-W, Duong T, Liao J-K (2013) The performance analysis of a real-time integrated INS/GPS vehicle navigation system with abnormal GPS measurement elimination. Sensors 13:10599–10622

Groves PD (2011) Shadow matching: a new GNSS positioning technique for urban canyons. J Navig 64:417–430. https://doi.org/10.1017/S0373463311000087

Groves PD (2013) Principles of GNSS, inertial, and multi-sensor integrated navigation systems (GNSS technology and applications), 2nd edn. Artech House Publishers, Boston

Groves PD, Jiang Z (2013) Height aiding, C/N_0 weighting and consistency checking for GNSS NLOS and multipath mitigation in urban areas. J Navig 66:653–669

Groves PD, Wang L, Adjrad M, Ellul C (2015) GNSS shadow matching: the challenges ahead. In: Proceedings of ION GNSS + 2015, Tampa, Florida, Sept 2015, pp 2421–2443

Gu Y, Hsu L-T, Kamijo S (2015) GNSS/on-board inertial sensor integration with the aid of 3D building map for lane-level vehicle self-localization in urban canyon. IEEE Trans Veh Technol 65:4274–4287

Han H, Wang J, Wang J, Tan X (2015) Performance analysis on carrier phase-based tightly-coupled GPS/BDS/INS integration in GNSS degraded and denied environments. Sensors 15:8685

Hartinger H, Brunner FK (1999) Variances of GPS phase observations: the SIGMA-ε model. GPS Solut 2(4):35–43

HKPSG (2016) Hong Kong planning standards and guidelines. Technical Services Section of Planning Department, Government of Hong Kong, Wan Chai

Hsu L-T, Jan S-S, Groves P, Kubo N (2015) Multipath mitigation and NLOS detection using vector tracking in urban environments. GPS Solut 19:249–262

Hsu L-T, Gu Y, Huang Y, Kamijo S (2016a) Urban pedestrian navigation using smartphone-based dead reckoning and 3D maps aided GNSS. IEEE Sens J 16:1281–1293

Hsu L-T, Gu Y, Kamijo S (2016b) 3D building model-based pedestrian positioning method using GPS/GLONASS/QZSS and its reliability calculation. GPS Solut 20:413–428

Hsu L-T, Tokura H, Kubo N, Gu Y, Kamijo S (2017) Multiple faulty GNSS measurement exclusion based on consistency check in urban canyons. IEEE Sens J 17(6):1909–1917

Isaacs JT, Irish AT, Quitin F, Madhow U, Hespanha JP Bayesian localization and mapping using GNSS SNR measurements. In: 2014 IEEE/ION position, location and navigation symposium—PLANS 2014, 5–8 May 2014, pp 445–451

Iwase T, Suzuki N, Watanabe Y (2013) Estimation and exclusion of multipath range error for robust positioning. GPS Solut 17:53–62

Jiang Z, Groves P (2014) NLOS GPS signal detection using a dual-polarisation antenna. GPS Solut 18:15–26

Kanwal N, Hurskainen H, Nurmi J (2010) Vector tracking loop design for degraded signal environment. In: Ubiquitous positioning indoor navigation and location based service, Kirkkonummi, Finland, 14–15 Oct 2010, pp 1–4

Kumar R, Petovello MG (2014) A novel GNSS positioning technique for improved accuracy in urban canyon scenarios using 3D city model. In: Proceedings of ION GNSS + 2014, Tampa, Florida, USA, 8–12 Sept 2014, pp 2139–2148

Li B, Cui W, Wang B (2015) A robust wireless sensor network localization algorithm in mixed LOS/NLOS scenario. Sensors 15:23536

Misra P, Enge P (2011) Global positioning system: signals, measurements, and performance. Ganga-Jamuna Press, Lincoln, p 01773

Miura S, Hsu LT, Chen F, Kamijo S (2015) GPS error correction with pseudorange evaluation using three-dimensional maps intelligent. IEEE Trans Transp syst 16:3104–3115

Peyraud S, Bétaille D, Renault S, Ortiz M, Mougel F, Meizel D, Peyret F (2013) About non-line-of-sight satellite detection and exclusion in a 3D map-aided localization algorithm. Sensors 13:829–847

Peyret F, Bétaille D, Carolina P, Toledo-Moreo R, Gómez-Skarmeta AF, Ortiz M (2014) GNSS autonomous localization: NLOS satellite detection based on 3-D maps. IEEE Robot Autom Mag 21:57–63

Sharawi MS, Akos DM, Aloi DN (2007) GPS C/N_0 estimation in the presence of interference and limited quantization levels. IEEE Trans Aerosp Electron Syst 43:227–238

Special-Committee-159 (2001) Minimum operational performance standards for global positioning system/wide area augmentation system airborne equipment. Document, DO-229C, RTCA

Sun D, Petovello MG, Cannon ME (2013) Ultratight GPS/reduced-IMU integration for land vehicle navigation. IEEE Trans Aerosp Electron Syst 49:1781–1791

Suzuki T, Kubo N (2013) Correcting GNSS multipath errors using a 3D surface model and particle filter. In: Proceedings of ION GNSS + 2013, Nashville, Tennessee, USA, 16–20 Sept 2013, pp 1583–1595

Veitsel VA, Zhdanov AV, Zhodzishsky MI (1998) The mitigation of multipath errors by strobe correlators in GPS/GLONASS receivers. GPS Solut 2:38–45

Wang JH, Gao Y (2010) Land vehicle dynamics-aided inertial navigation. IEEE Trans Aerosp Electron Syst 46:1638–1653

Wang L, Groves P, Ziebart M (2012) Multi-constellation gnss performance evaluation for urban canyons using large virtual reality city models. J Navig 65:459–476

Wang L, Groves PD, Ziebart MK (2013) GNSS shadow matching: improving urban positioning accuracy using a 3D city model with optimized visibility scoring scheme. Navigation 60:195–207

Wang L, Groves PD, Ziebart MK (2015) Smartphone shadow matching for better cross-street GNSS positioning in urban environments. J Navig 68:411–433

Yozevitch R, Ben-Moshe B (2015) A robust shadow matching algorithm for GNSS positioning. Navigation 62:95–109

Yozevitch R, Ben-Moshe B, Dvir A (2014) GNSS accuracy improvement using rapid shadow transitions. IEEE Trans Intell Transp Syst 15:1113–1122

Yozevitch R, Ben-Moshe B, Weissman A (2016) A robust GNSS LOS/NLOS signal classifier. Navigation 63:429–442

Zhdanov A, Zhodzishsky M, Veitsel V, Ashjaee J (2002) Evolution of multipath error reduction with signal processing. GPS Solut 5:19–28

Li-Ta Hsu received the B.S. and Ph.D. degrees in aeronautics and astronautics from National Cheng Kung University, Taiwan, in 2007 and 2013, respectively. He is currently an assistant professor with Interdisciplinary Division of Aeronautical and Aviation Engineering, The Hong Kong Polytechnic University, before he served as post-doctoral researcher in Institute of Industrial Science at University of Tokyo, Japan. In 2012, he was a visiting scholar in University College London, U.K. His research interests include GNSS positioning in challenging environments and localization for autonomous driving vehicle and unmanned aerial vehicle.